GASDYNAMIC MECHANISM OF PRESSURE LIMITATION BEHIND FOCUSING SHOCK WAVES

A. V. Potapkin and Yu. N. Yudintsev

UDC 533.6:519.6

In many gasdynamic phenomena one must analyze the behavior of shock waves (SW) with fronts concave in the direction of propagation. The propagation of such SW is accompanied by an increase in their intensity, the maximum of which is reached in the region defined as the focusing zone. In the case of weak SW, the Mach number of which is $M_w \approx 1.0$, the simplest description of the dynamics of fronts concave in the direction of propagation can be made on the basis of geometrical acoustics [1]. In accordance with geometrical acoustics, SW emerge from the geometrical focus in the form of intersecting "loop-shaped" fronts. A feature of geometrical acoustics is that it does not allow for nonlinearity in the velocity of propagation of the wave fronts as the SW strengthen in the process of focusing, and it predicts an unlimited increase in SW intensity at the envelopes of acoustic rays (caustics). The theory of [2] gives a qualitatively different picture of the dynamics for SW of moderate intensity. The strengthening of SW sections concave in the direction of propagation and the weakening of convex sections result in the fact that different sections of the SW front propagate at different velocities. Straightening of the SW front occurs, the trajectories of motion of elements of the front become curved and do not intersect, and the SW intensity remains finite.

Experimental investigations of the dynamics of SW with fronts concave in the direction of propagation [3] made it possible to distinguish the main types of SW configurations in the focusing zone. On the basis of an analysis of straight-shadow photographs of the structure of gas flow behind the SW and measurement of the pressure in the field behind the SW front, it was concluded that the limitation of the intensity of such SW during focusing is accomplished through the decrease in pressure in rarefaction waves propagating along the front of the focusing SW. The focusing of weak SW was studied analytically in [4]. The problem was reduced to the solution of the wave equation in a specially deformed coordinate system. It was concluded that the reason for the limitation of the intensity growth of focusing SW is the refraction of the SW. A defect of the work is the strong restriction imposed on the shape of the SW fronts.

In the present work the dynamics of shock waves was investigated numerically on the example of two problems of the propagation of SW with concave fronts in an unbounded space and in a channel with rigid walls. As the initial system we took a system of two-dimensional, nonsteady equations of gasdynamics describing the motion of an inviscid and thermally nonconducting gas in regions of space where the parameters of the gas are continuous:

$$\partial \bar{a}/\partial t + \partial \bar{b}/\partial x + \partial \bar{c}/\partial y = -\nu \bar{d}/y.$$

Here

$$\bar{a} = \begin{bmatrix} \rho \\ \rho u \\ \rho v \\ e_0 \end{bmatrix}; \quad \bar{b} = \begin{bmatrix} \rho u \\ p + \rho u^2 \\ \rho uv \\ (e_0 + p)u \end{bmatrix}; \quad \bar{c} = \begin{bmatrix} \rho v \\ \rho uv \\ p + \rho v^2 \\ (e_0 + p)v \end{bmatrix}; \quad \bar{d} = \begin{bmatrix} \rho v \\ \rho uv \\ \rho v^2 \\ (e_0 + p)v \end{bmatrix};$$

t is time; x and y, orthogonal coordinates; ρ, gas density; u and v, components of the gas velocity along x and y, respectively; p, gas pressure; $e_0 = \rho e + \rho(u^2 + v^2)/2$, total energy of the gas. The system of equations was closed by the equation of state of a polytropic gas, $e = p/[(\gamma - 1)\rho]$ (γ is the adiabatic index of the gas, taken as 1.4 in the calculations). The parameter ν took values of 0 and 1, which correspond to plane and axial symmetry. The system of equations was solved in the moving region D, traveling in the space xOy (Fig. 1).

Novosibirsk. Translated from Zhurnal Prikladnoi Mekhaniki i Tekhnicheskoi Fiziki, No. 2, pp. 119-125, March-April, 1986. Original article submitted September 3, 1984.

0021-8944/86/2702-0267$12.50

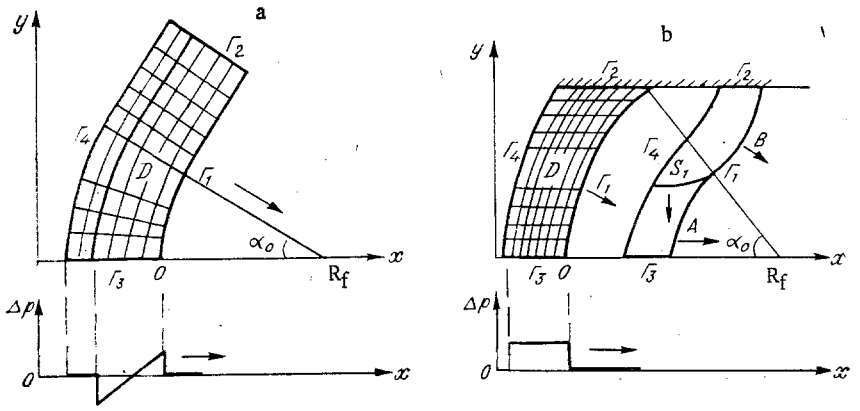

Fig. 1

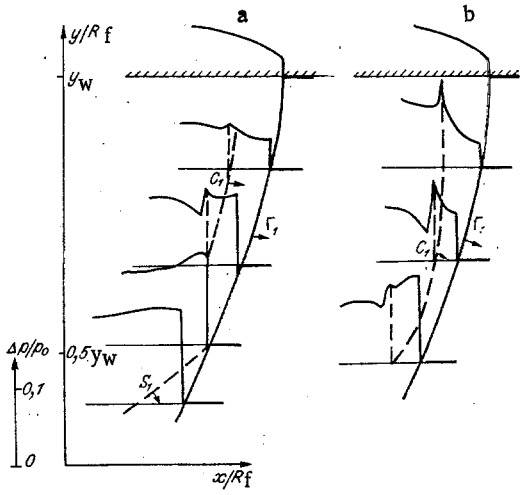

Fig. 2

The configuration of the region with the elapse of time was determined by the motion of the boundaries. The following were assigned as the boundaries of the calculation region: the SW front Γ_1; the axis (plane) of symmetry Γ_3; a boundary Γ_2 in the gas stream, displaced sufficiently far from Γ_3 (Fig. 1a), or the rigid wall of the pipe (channel) (Fig. 1b); the moving surface Γ_4 behind the trailing shock (Fig. 1a) or a certain surface traveling behind Γ_1 [Fig. 1b, where A is the focusing section of the shock wave Γ_1, B is the diffracted SW, and S_1 is the front of the rarefaction flow propagating from the wall toward the axis (plane) of symmetry]. All the parameters of the gas in the region D were determined at the initial time. For the flow geometry shown in Fig. 1a, the pressure at the SW is constant along Γ_1 and the profile of the rarefaction wave is linear along the normal to Γ_1. In the case shown in Fig. 1b it was assumed that Γ_1 at the initial time is a spherical (cylindrical) diaphragm separating two states of a stationary gas. Here it was assumed that the gas pressure behind the diaphragm Γ_1 is higher than the pressure ahead of it and the gas temperature is the same everywhere. The gas parameters ahead of the SW front were assigned as constants.

Following the instantaneous removal of the diaphragm, a shock wave Γ_1 with a curved front propagates through the gas to the right. It was required that the conditions of a shock transition be satisfied at Γ_1 , the condition of symmetry of the gas stream relative to Γ_3 was set up at this boundary, the condition of nonpenetration at the solid wall, and the condition $\partial\psi/\partial\bar{n} = 0$ (ψ is any parameter of the gas and $\bar{n}$ is the outward normal to the boundary Γ_2) at the boundary Γ_2 (Fig. 1a). The same condition was set up at Γ_4 for the first problem, while for the second problem (Fig. 1b) it was required that the normal velocity of travel of Γ_4 be no lower than the velocity of propagation of local disturbances in the gas stream ahead of Γ_4, which enabled us to assign the gas parameters at Γ_4 which were calculated in the stream ahead of Γ_4.

The numerical algorithm for solving the stated problems is based on an explicit difference scheme [5] in a moving difference grid, connected with the shock wave front Γ_1 explicitly isolated in the process of calculation. The calculation algorithm is described in [6], while the results of parametric research are contained in [7]. In the calculations of flows in pipes (channels) (Fig. 1b) we used nonuniform difference grids, adjusted to the flow structure and providing an acceptable calculation accuracy [8].

As experimental [3] and numerical research [7] showed, the main parameters determining the behavior of the SW intensity in the focus zone are the angle of convergence α_0 of the SW (see Fig. 1) and its initial relative intensity $\Delta p_0/p_0$ (p_0 is the pressure in the gas ahead of Γ_1 and Δp_0 is the initial amplitude of the excess pressure at the SW).

The presence of a point of discontinuity of the curvature of the front (a) or of a rigid wall in the gas stream (b) at the initial SW leads to the formation of disturbances propagating along the front Γ_1. The experimental results of [3] point to a direct dependence of the process of focusing of the SW on the flow structure behind it. Therefore, a number of calculations were made in order to clarify the properties of gas flow behind a focusing SW. In Fig. 2 we present fragments of the flow behind the SW near the pipe wall for the initial parameters $\Delta p_0/p_0 = 0.1$ and $\alpha_0 = 30°$; the positions of Γ_1 are shown for the values $x/R_f = 0.3$ and 0.42 (a, b), where R_f is the focal length (see Fig. 1) and y_w is the coordinate of the wall. The pressure profiles behind Γ_1 in the Ox direction are given. The position of the front S_1 of the rarefaction wave propagating from the wall toward the axis of symmetry is given for $x/R_f = 0.3$. The reason for the appearance of rarefaction flow is the diffraction of Γ_1 on the wall, as a result of which the SW becomes convex in the direction of propagation near the wall. The pressure profiles indicate the formation of a compression wave C_1 propagating behind Γ_1. The appearance of the compression wave is explained by the reflection of the rarefaction wave from the SW Γ_1. The rarefaction and compression waves behind the front Γ_1 play a pronounced role in equalizing the pressure along Γ_1. The SW intensity is decreased by the rarefaction waves, but the intensity of Γ_1 increases in the wall region because of compression waves overtaking the SW.

A discontinuity in the curvature of the initial front also leads to the formation of rarefaction flow along the focusing section of the SW.

For weak SW ($\Delta p_0 \ll p_0$) the nonlinearity of the focusing process is well traced in the numerical calculations. In Fig. 3 we present the amplification ratio $k = \Delta p/\Delta p_0$ of the SW, the radius of curvature R_C of the front, and the acceleration W of the SW at the axis of symmetry as functions of the distance traveled by the SW in the direction toward the geometrical focus (for the case shown in Fig. 1b). The point $x/R_f = 0$ corresponds to the initial position of the SW while $x/R_f = 1$ corresponds to the geometrical focus; lines 1) solution of geometrical acoustics; 2-5) numerical solutions obtained for $\alpha_0 = 8°$ and $\Delta p_0/p_0 = 0.1$; $\alpha_0 = 12°$ and $\Delta p_0/p_0 = 0.1$; $\alpha_0 = 16°$ and $\Delta p_0/p_0 = 0.1$; and $\alpha_0 = 16°$ and $\Delta p_0/p_0 = 0.05$, respectively.

The behavior of curves 2-5 indicates that the processes of SW focusing for the given parameters α_0 and $\Delta p_0/p_0$ occur with the same character. It is seen from Fig. 3 that, starting with certain values of x/R_f, curves 2-5 diverge from lines 1 and W takes the maximum value here. An analysis of the flow fields showed that at these times the front S_1 of the rarefaction flow reaches the axis of symmetry in propagating along the front Γ_1. In the further propagation of the shock waves, the amplification ratio k reaches the maximum value, while $W = 0$. Thus, the entire focusing process can be divided into a number of successive stages. The first stage begins at the initial time and ends when S_1 reaches the axis of symmetry while the shock wave Γ_1 has not yet arrived at the geometrical focus, which is a consequence of the nonlinearity in the propagation of disturbances behind the front of a focusing shock. The coincidence of curves 2-5 with lines 1 (see Fig. 3a, b) in this stage indicates that the process of strengthening of the section of the shock wave Γ_1 lying between S_1 and the axis of symmetry takes place in accordance with geometrical acoustics. From the time of arrival of S_1 at the axis of symmetry, the second stage begins, and it ends in the zone of the maximum value of the amplification ratio. The behavior of curves 2-5 in Fig. 3b indicates that from this time the radius of curvature R_C of the SW front at the axis of symmetry grows rapidly and becomes infinitely large, i.e., straightening of the SW front occurs and the wave becomes plane at the axis of symmetry.

An analysis of the flow fields behind Γ_1 and of the distributions of $\alpha(y)$ and $\Delta p/p_0$ along the front Γ_1 showed that the formation of a Mach SW configuration occurs in this stage [$\alpha(y)$

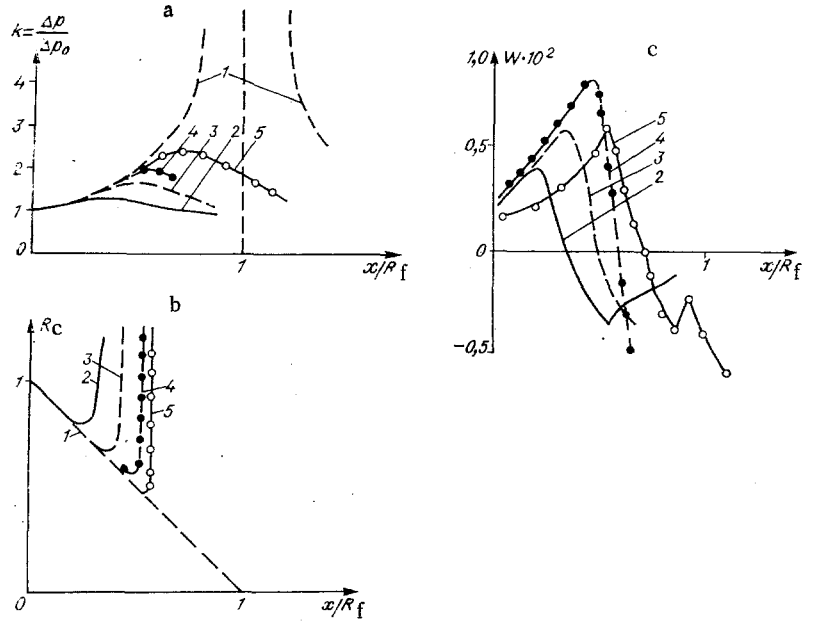

Fig. 3

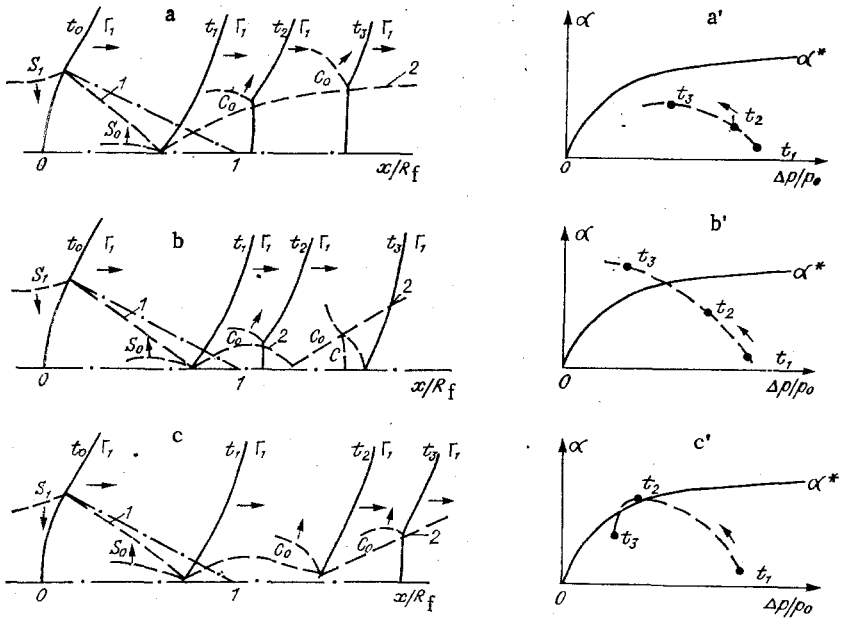

Fig. 4

is the angle between the Oy axis and the tangent to the shock wave front Γ_1]. From Fig. 3a it is seen that in the stage of formation of the Mach SW configuration, the SW intensity at the axis of symmetry continues to grow. Such behavior of the amplification ratio is explained by the peculiarities of Mach reflection of SW under nonsteady conditions. The reflection coefficient in a Mach SW configuration is determined by the angle of inclination and the intensity of the incident SW. In our case, an incident SW and a Mach stem can be distinguished in the SW from the time of arrival of S_1 at the axis of symmetry. The disturbances propagating along the incident wave form the intensity distribution and the angle of inclination $\alpha(y)$ of the shock front, which in turn determines the coefficient of reflection of the SW at the axis of symmetry.

Thus, there are two nonlinear processes occurring simultaneously. In the problems under consideration, there is a decrease in the intensity of the incident SW because of the lowering of pressure by rarefaction waves, while on the other hand the intensity of the Mach stem near the axis of symmetry grows because of the increase in the angle of inclination of the incident

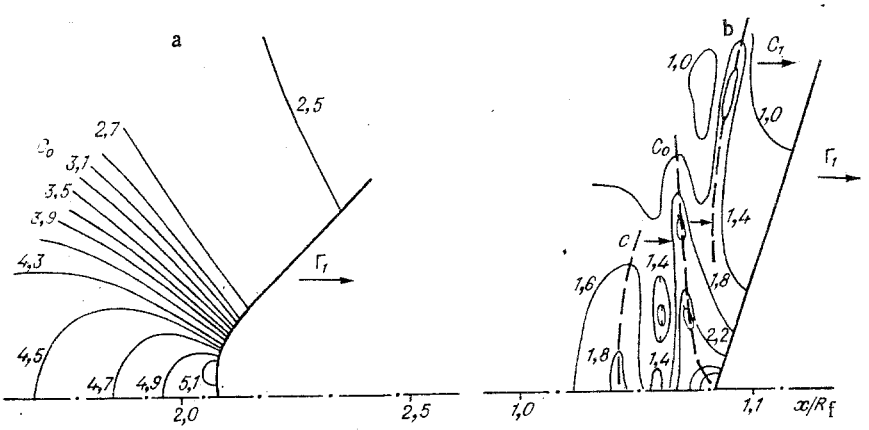

Fig. 5

shock. The proportion of these two processes determines the behavior of the amplification ratio k, which increases if the SW reflection coefficient grows faster than the intensity of the incident SW is lowered by the rarefaction waves. The results presented in Fig. 3 confirm that the length of this stage of SW strengthening depends on the initial parameters of the problem ($\Delta p_0/p_0$ and α_0). For example, a comparison of curves 2-4 shows that the length of the stage of SW strengthening during the formation of the Mach configuration can be prolonged if the angle of convergence α_0 is reduced for a fixed value of $\Delta p_0/p_0$ or $\Delta p_0/p_0$ is reduced for a fixed α_0 (from a comparison of curves 4 and 5).

Thus, from the results of numerical calculations it is concluded that in the second stage of the focusing process the SW intensity in the focal zone is determined by the structure of the Mach reflection of the SW. As follows from the experimental data of [3], however, wave structures with regular interaction of the SW can develop behind the focusing zone, depending on the initial SW parameters. Such a variety of structures in the focusing zone and behind it is explained, as above, by the peculiarities of nonsteady reflection of SW from the axis of symmetry. In Fig. 4a-c we present diagrams of wave structures, constructed from the results of the calculations and the experiments of [3], with variation of the initial parameters of the focusing shock: line 1) trajectory of the point of intersection of the shock wave front Γ_1 with the front of the disturbance S_1 propagating along Γ_1; S_0) front of the disturbance after reflection from the axis of symmetry; 2) trajectory of the triple point; C_0) reflected shock wave; C) compression wave behind the reflected shock wave C_0. Common to these diagrams is the formation of a Mach SW configuration at the time t_1 when the front S_1 of the disturbance wave reaches the axis of symmetry; with the course of time, this reflection pattern can be retained and developed (a), it can change into a scheme with regular reflection of the shock wave Γ_1 (b), or an intermediate wave structure can develop (c).

The transition from Mach reflection to regular reflection and vice versa occurs at critical angles of inclination of the incident shock, the value of which depends on the shock intensity $\Delta p/p_0$. The values of the critical angles for the reflection of weak SW from a rigid wedge were determined experimentally and analytically in [9, 10]. In Fig. 4a'-c' the dependence of the critical angle α^* on $\Delta p/p_0$ is represented schematically and the possible behavior of the angle of inclination and the intensity of the incident shock Γ_1 in the process of reflection are shown for each of these schemes. Here the region of $\alpha < \alpha^*$ corresponds to the region of existence of Mach reflection, while regular reflection occurs for $\alpha > \alpha^*$. The times t_1, t_2, and t_3 correspond to the positions of the shocks in the diagrams on the left. As already mentioned, in the process of focusing, the intensity and the angle of inclination of the incident shock vary under the action of disturbances propagating along the front of the shock Γ_1. A Mach configuration of shocks is formed at the time t_1, since the angle of incidence α is close to zero, as is shown in Fig. 4. Subsequently, if the angle of incidence remains less than the critical value α^*, a Mach SW configuration always exists, as in Fig. 4a. The applicability of the theory of shock dynamics of [2] for calculating the Mach reflection of SW of moderate intensity was confirmed experimentally in [11]. Hence it follows that the focusing of SW of moderate intensity ($\Delta p_0 \approx p_0$) will also be described well by this theory.

If the angle of inclination of the incident shock grows rapidly in the process of reflection, which occurs for large angles of convergence, then the Mach configuration starts to degenerate into the regular scheme of reflection, which originates and develops from the time corresponding to $\alpha > \alpha^*$ (Fig. 4b).

Finally, an intermediate wave structure, which has been detected experimentally [3], is also possible. Here the stage of regeneration of the Mach configuration into the regular configuration is not finished, since the curve of the dependence $\alpha(\Delta p/p_0)$ for the incident shock after the time t_2 returns to the region of existence of the Mach shock configuration (Fig. 4c).

To illustrate the proposed schemes, in Fig. 5 we present fields of isobars behind the shock wave Γ_1, constructed from the calculated results. In Fig. 5a we present a typical pattern of a Mach SW configuration (it corresponds to Fig. 4a, $\Delta p_0/p_0 = 1.5$, $\alpha_0 = 45°$ [6]) developing after the passage of the shock wave Γ_1 far behind the geometrical focus. The incident wave and the Mach wave are clearly distinguished (front Γ_1), while the position of the reflected wave C_0 is defined by the bunching of the isolines of $\Delta p/p_0 = \text{const}$. Figure 5b corresponds to Fig. 4b with the initial parameters $\Delta p_0/p_0 = 10^{-2}$ and $\alpha_0 = 20°$. The behavior of the isolines of $10^2\Delta p/p_0 = \text{const}$ enables one to determine the position of the reflected wave C_0 in the pattern of regular reflection, the position of the shock C_1 formed behind Γ_1 as a result of the reflection of the rarefaction wave from the shock wave Γ_1 (see Fig. 2), and the compression wave C. The flow pattern is identified by dashed lines.

We have examined the peculiarities of the behavior of the amplitude of focusing SW and the wave configurations in the focusing zone for the simplest cases of concave fronts with a constant initial curvature and intensity. In actual situations, the causes of the development of concave fronts can be quite varied (stream nonuniformity, refraction, reflection, nonsteadiness of propagation, etc.), but their dynamics in the process of focusing will contain those basic elements discussed above.

LITERATURE CITED

1. F. G. Friedlander, Sound Pulses, Cambridge University Press, England (1985).
2. G. B. Whitham, "A new approach to problems of shock dynamics. Part 1. Two-dimensional problems," J. Fluid Mech., 2, No. 2 (1957).
3. B. Sturtevant and V. A. Kulkarny, "The focusing of weak shock waves," J. Fluid Mech., 73, No. 4 (1976).
4. F. Obermeier, "On the propagation of weak and moderately strong, curved shock waves," J. Fluid Mech., 129 (1983).
5. S. K. Godunov (ed.), Numerical Solution of Multidimensional Problems of Gasdynamics [in Russian], Nauka, Moscow (1976).
6. A. V. Potapkin and A. I. Rudakov, "Numerical approach to the investigation of focusing of shock waves," Mezhvuz. Sb. Krasnoyarsk (1979).
7. A. V. Potapkin, A. I. Rudakov, and Yu. N. Yudintsev, "Numerical investigation of the focusing of shock waves," Chislennye Metody Mekh. Splosh. Sredy, 10, No. 3 (1979).
8. A. V. Potapkin, "Use of bunching grids in calculations of flows with large gradients," Chislennye Metody Mekh. Splosh. Sredy, 14, No. 3 (1983).
9. O. S. Ryzhov and S. A. Khristianovich, "Nonlinear reflection of weak shock waves," Prikl. Mat. Mekh., 22, No. 5 (1958).
10. B. I. Zaslavskii and R. A. Safarov, "Similarity of flows arising in the reflection of weak shock waves from a rigid wall and a free surface," Fiz. Goreniya Vzryva, 9, No. 4 (1973).
11. T. V. Bazhenova and L. G. Gvozdeva, Nonsteady Interactions of Shock Waves [in Russian], Nauka, Moscow (1977).